International Journal of Thermophysics, Vol. 19, No. 3, 1998

Phase Diagram and Free Energies of Vapor Films and Tubes for a Confined Fluid[1]

K. Lum[2] and D. Chandler[2, 3]

When confined between two parallel drying surfaces that are separated by a small distance, D, a liquid close to liquid-gas coexistence becomes metastable and evaporates. This paper focuses on this surface-induced phase transition. With mean field theory, we describe the pertinent phases and the corresponding density profiles for a lattice gas model. In one of the three phases, vapor films form between the liquid and the drying surfaces. Analytical estimates and Monte Carlo simulations indicated that the pathway to evaporation involves the concerted action of high-amplitude fluctuations of the vapor–film interfaces and the formation of vapor tubes that bridge these interfaces.

KEY WORDS: confined fluid; drying surfaces; evaporation; interfaces.

1. INTRODUCTION

When a liquid is in equilibrium with its vapor in the presence of a surface, the liquid–gas interface is characterized in part by the angle it makes with the surface. This contact angle, θ_c, is determined by the interfacial energetics through the Young–Dupré equation, $\sigma_{sg} - \sigma_{sl} = \sigma_{gl} \cos \theta_c$, where σ_{sl}, σ_{sg}, and σ_{gl} are the surface–liquid, the surface–gas, and the gas–liquid surface tensions, respectively. For a drying surface, $\sigma_{sl} > \sigma_{sg}$, and thus the contact angle θ_c is greater than 90°. When a pair of drying surfaces are arranged in parallel at a separation D and immersed in the liquid, the

[1] Paper presented at the Thirteenth Symposium on Thermophysical Properties, June 22–27, 1997, Boulder, Colorado, U.S.A.

[2] Department of Chemistry, University of California at Berkeley, Berkeley, California 94720, U.S.A.

[3] To whom correspondence should be addressed.

0195-928X/98/0500-0845$15.00/0 © 1998 Plenum Publishing Corporation

liquid between these surfaces may evaporate. This example of a surface-induced phase transition occurs when the grand canonical free energies of the confined liquid ($\Omega_l \sim -pV + 2A\sigma_{sl}$) and the confined gas ($\Omega_g \sim -p_g V + 2A\sigma_{sg}$) are comparable [1, 2]. Here, p is the bulk pressure and p_g is the pressure of the coexisting vapor, and the volume of the confined region is $V = AD$.

The critical separation at which the confined vapor becomes thermodynamically favorable is then given by

$$D_c \sim -\frac{2\sigma_{gl}\cos\theta_c}{(p-p_g)} = -\frac{2\sigma_{gl}\cos\theta_c}{\rho_l \Delta\mu} \tag{1}$$

The second equality is obtained for an incompressible fluid by approximating $p - p_g$ by $\rho_l \Delta\mu$, where ρ_l is the liquid density and $\Delta\mu$ is the difference of the chemical potential of the bulk liquid from liquid–gas coexistence. This relationship is analogous to the Kelvin equation for capillary condensation. When σ_{gl} is not small, but $\Delta\mu$ is small, D_c can be a very large length. For instance, water at normal conditions is close to liquid–gas coexistence. The resulting $\Delta\mu$ is so small that $D_c \sim 10^3$ Å in that case. This paper is concerned with the formation of interfaces and the kinetic pathway of this surface-induced transition.

In experiments measuring forces between two hydrophobic surfaces in water [3, 4], at separations of about 100 Å, the two surfaces jump into contact. Additionally, the forces exhibit hysteresis in the inward and outward going measurements, suggesting possible metastabilities associated with first-order phase transitions. In analogous experiments [5], phase separations of confined binary ($\alpha\beta$) liquid mixture have also been investigated. The solute species β is sparingly soluble in liquid α. Two surfaces that favor the β species are allowed to approach in the slightly undersaturated solution. A sudden inward jump of the surfaces (toward each other) and condensation of the β-phase between the surfaces are observed.

Yaminsky et al. [6] suggested that the mechanism for the surface-induced evaporation involves the formation of a vapor tube across the two surfaces. When the vapor tube grows to a critical size, the metastable liquid loses stability and evaporates. However, from the free energy for nucleating a critical vapor tube,[4] one would predict that the time scale for evaporation is far too long to observe in any physically accessible time. Yet, the evaporation can be observed during the course of a relatively short Monte Carlo trajectory [7]. Therefore, the pathway to evaporation

[4] From standard surface thermodynamics, the free energy to form a vapor tube of radius r is $2\pi rD\sigma_{gl} + 2\pi r^2(\sigma_{sg} + \sigma_{sl})$. The free energy for forming a vapor tube of critical size is then $\pi D^2\sigma_{gl}/2\cos\theta_c (\sim 180 k_B T$ for $D = 10$ Å, $\sigma_{lg} = 70$ dyne cm^{-1}, $\theta_c = 180°$, and $T = 298$ K).

involves something different than simply tube formation. Before focusing on the pathway, it is useful to begin by considering the interfacial phase diagram associated with the phenomenon.

2. MEAN FIELD THEORY OF LATTICE GAS MODEL FOR CONFINED FLUIDS

The lattice gas Hamiltonian is given by

$$\mathscr{H}[\{n_i\}] = -\varepsilon \sum_{\langle ij \rangle} n_i n_j - \varepsilon_s \sum_{i \in \text{surface}} n_i - \mu \sum_i n_i \tag{2}$$

where ε is the nearest-neighbor interaction, ε_s is the surface-particle interaction, μ is the chemical potential, and $n_i (=0, 1)$ is the occupation number for the ith cell in a cubic lattice. Confining surfaces bound the system at $z=0$ and $z=D+1$. The first sum runs over all nearest-neighbor pairs. The second sum runs over all sites next to the surfaces. Phase behavior of lattice-gas models in the presence of surfaces has been studied within the mean-field approximation [8–10] and by simulations [11–14]. Here, we are concerned with the phase diagram in terms of the bulk and the surface fields.

Below the critical temperature, T_c, the system in bulk (i.e., without surfaces) phase separates into two phases with average densities ρ_l and ρ_g $(=1-\rho_l)$ at $\mu_{coex} = -\zeta\varepsilon/2$, where ζ is the number of nearest neighbors. In the presence of confining surfaces, the phase coexistence is shifted to

$$\Delta\mu = \mu - \mu_{coex} = (\zeta_\perp \varepsilon - 2\varepsilon_s)/D \tag{3}$$

where $\zeta_\perp$ is the number of nearest neighbor in the adjacent layer (for cubic lattice, $\zeta = 6, \zeta_\perp = 1$). This relationship is the low-temperature approximation to Eq. (1). It describes a phase transition that occurs when the liquid is in contact with the drying surfaces.

Alternatively, an evaporation transition can occur from a phase of the confined fluid where a vapor film lies between the liquid and each drying surface. The vapor film is formed from a predrying transition [9, 15]. It occurs when the surface-particle attraction is so small that the attraction from the bulk effectively pushes the particle away from the surface [16], leaving a region of low occupancy next to the surface. The density away from the surface rises to its bulk liquid density ρ_l at the given (μ, ε). In the low-temperature limit, the predrying line is given by

$$(\zeta_\perp \varepsilon - 2\varepsilon_s) = 2\,\Delta\mu - \varepsilon(2\rho_l - 1) \tag{4}$$

Because of the discreteness of the underlying lattice, the interface between the low-density and the high-density phases in this model undergoes a roughening transition at temperature T_R [17]. This roughening transition is not relevant to liquid-gas interfaces in real fluids, and in all our considerations, $T_R < T < T_c$.

In the vapor–film phase, as the intersurface separation decreases, the stability gained by the liquid film cannot support the liquid–gas interfaces, and the system becomes metastable with respect to the gas state. From the same considerations that lead to Eq. (3), evaporation of the vapor film is predicted to occur when $\Delta\mu = 2\sigma_{gl}/(D - 2\bar{\ell})$ [2], where $\bar{\ell}$ is the average thickness of the vapor film. At low temperature where the liquid–gas interface is sharp and fluctuations can be neglected, the shift in coexistence can be approximated by

$$\Delta\mu = \varepsilon/(D-2) \tag{5}$$

The above-mentioned phase transitions can be predicted on the mean field level. The free energy of the lattice-gas model is

$$F = -k_B T \log \sum_{\{n_i\}} \exp(-\beta \mathcal{H}[\{n_i\}]) \tag{6}$$

where k_B is Boltzmann's constant and $\beta = 1/k_B T$. Assuming translational invariance in the x–y plane, the mean-field approximation for the free energy and the average density profile, $\langle n_z \rangle$, can be obtained by minimizing the functional [8–10],

$$\begin{aligned} F[\langle n_z \rangle]/A = {} & \frac{-\varepsilon(\zeta - 2\zeta_\perp)}{2} \sum_{z=1}^{D} \langle n_z \rangle^2 - \zeta_\perp \varepsilon \sum_{z=1}^{D-1} \langle n_z \rangle \langle n_{z+1} \rangle \\ & - \varepsilon_s \sum_{z=1,D} \langle n_z \rangle - \mu \sum_{z=1}^{D} \langle n_z \rangle \\ & + k_B T \sum_{z=1}^{D} [\langle n_z \rangle \log\langle n_z \rangle + (1 - \langle n_z \rangle) \log(1 - \langle n_z \rangle)] \end{aligned} \tag{7}$$

The phase diagram for $\beta\varepsilon = 1.652$ is calculated numerically and shown in Fig. 1. The symbols ($\square$, $\diamond$, and $\triangle$) denote the locations at which coexistence occurs. The triple point, denoted by $\bullet$, is where the three phases coexist. The dotted lines are the low temperature limit given by Eqs. (3)–(5). In this limit, a triple point is located at $\Delta\mu = \varepsilon/(D-2)$, $(\zeta_\perp \varepsilon - 2\varepsilon_s) = D\varepsilon/(D-2)$.

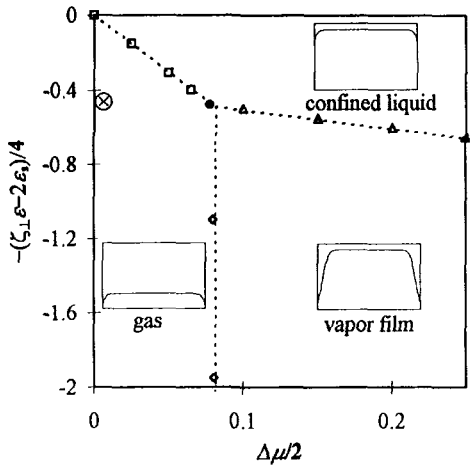

Fig. 1. The mean field phase diagram as a function of the bulk and surface field at $\beta\varepsilon = 1.652$. Three phases are identified. The dotted lines are estimates from low-temperature position of the lattice-gas systems we simulated. Insets are schematic depictions of the corresponding density profiles, $\langle n_z \rangle$. From Eq. (3), the slope of the line of coexistence between the confined liquid and the gas states varies with the surface separation as $-D$. From Eq. (5), the distance between the line of vapor film–gas coexistence and the line for $\Delta\mu = 0$ varies with the surface separation as $1/(D-2)$. As $D \to \infty$, the phase boundaries for the gas state merge with the line for $\Delta\mu = 0$.

As interfacial profiles are more diffuse at high temperatures and small $\Delta\mu$, the agreement with the low-temperature predictions becomes less satisfactory as we raise the temperature. This fact is illustrated in Fig. 2 where the phase diagram for $\beta\varepsilon = 0.976$ is shown. Indeed, the deviation is more pronounced as $\Delta\mu$ decreases, and the vapor–film state is more stable than predicted from sharp interfaces. The predrying line in Fig. 2 ends at a critical point. The critical behavior at $\beta\varepsilon > \beta_c\varepsilon$ ($=4/\zeta$ classically) originates from the mean field equation satisfied by the density at $z = 1, D$,

$$2\langle n_z \rangle - 1 = \tanh\left[\frac{\beta\varepsilon(\zeta - 2\zeta_\perp)}{4}(2\langle n_z \rangle - 1) + \beta\varepsilon\zeta_\perp\langle n_{z'} \rangle + \beta\varepsilon_s + \beta\mu\right] \tag{8}$$

where $z' = 2, D-1$, for $z = 1, D$, respectively. When $\beta\varepsilon < 4/(\zeta - 2\zeta_\perp)$, as the system approaches the critical point along the predrying line, the jump in

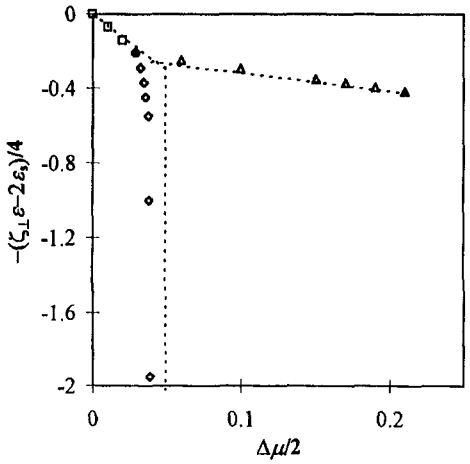

Fig. 2. The mean-field phase diagram as a function of the bulk and surface field at $\beta\varepsilon = 0.976$. The line of coexistence between the liquid and the vapor–film state ends at a critical point at about $\Delta\mu/2 = 0.21$ and $(\zeta_\perp\varepsilon - 2\varepsilon)/4 = -0.42$.

surface densities between the two states vanishes. The critical point moves toward the triple point as temperature increases. When the two points merge, the system can be found in only two thermodynamically stable states, namely, the gas state and the high-density state. The predrying transition can be observed only as a transition between metastable states in the gas region.

3. THE PATHWAY TO EVAPORATION

We now turn to the dynamics of the confinement induced evaporation. Since the vapor–film state contains two liquid–gas interfaces, the dynamics may involve interfacial capillary-wave fluctuations [18, 19]. These fluctuations are suppressed in the presence of a large bulk field, $\Delta\mu$. For systems close to coexistence, however, these fluctuations cannot be neglected. Due to the long-wavelength nature of capillary waves, one must account for large system size.

Figure 3 shows a cross section of a nascent configuration in the Monte Carlo simulation of a confined lattice gas [7]. The lateral dimension of the $L \times L \times D$ system is much longer than the separation between the confining surfaces ($L = 512$ and $D = 12$). Capillary waves are evident in the figure. Where the two interfaces approach one and other, vapor tubes may bridge

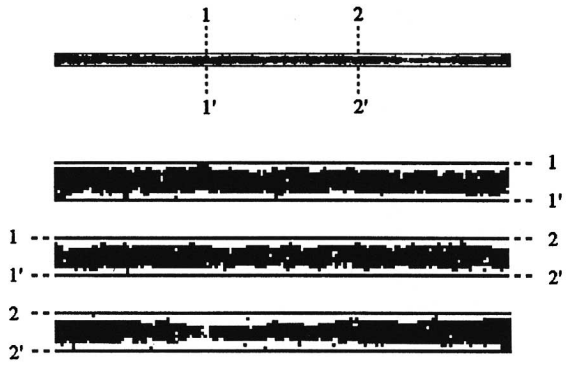

Fig. 3. (a) Cross section of the $L \times L \times D$ lattice gas system ($L = 512$ and $D = 12$) at about 10,000 passes. The straight lines at the top and the bottom represent the drying surfaces. Cells are black when occupied, and white when empty. In b, the cross section is divided and enlarged to show the features more clearly. The particular vapor tube seen here not grow to its critical size but, instead, disappeared at a later simulation step. The vapor tubes are not confined to the center of the system. This system is not to be confused with lattice-gas simulation in a cylindrical pore geometry (e.g., Ref. 20), in which the third dimension is small ($\sim D$) and bounded.

the interfaces. One such tube is seen in Fig. 3. The boundary conditions in the lateral direction are defined to mimic a liquid reservoir outside the confined region ($n_i = 1$ at the boundary in the lateral direction). These fixed boundary conditions pin the interfaces at the edges.

To examine the equilibrium phase transition properties, others [11–14] have simulated lattice-gas models of confined fluids in slit geometries, as we have done. But in these other works, the lateral size, L, has not been much larger than the separation between surfaces, D, and periodic boundary conditions have been applied parallel to the surfaces. The lateral size and boundary conditions are, however, crucial in determining the dynamics of the system, as we discuss now.

The lattice-gas parameters used in our simulation are $\beta\varepsilon = 1.653$, $\beta\varepsilon_s = 0.01$, $\beta\Delta\mu = 0.0002589$, and $a = 2.2$ Å. These parameters are chosen such that the corresponding lattice-gas system exhibits high surface tension, close proximity to vapor–liquid coexistence, and high incompressibility. With the given parameters, the system is located in the gas region of the phase diagram, indicated by $\otimes$ in Fig. 1. Using Glauber dynamics, and the liquid phase as initial conditions, the time evolution of the grand canonical lattice-gas system to its ultimately stable gas phase is followed.

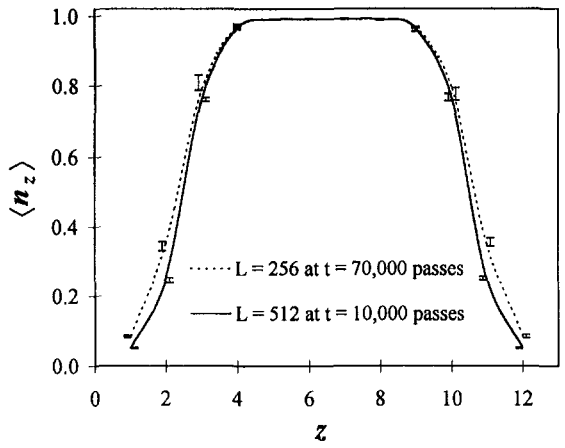

Fig. 4. Density profiles $\langle n_z \rangle$ from Monte Carlo simulations on lattice-gas systems ($D = 12$, $L = 256, 512$). The smoothed curves are symmetrized averages over $\langle n_z \rangle$ at 10 simulation times separated by 100 passes, i.e., at $t - 900$, $t - 800$,..., $t - 100$, t passes. The bars, unsymmetrized, show the range of density fluctuations over this time interval.

The configuration illustrated in Fig. 3 is obtained after 10,000 passes (1 pass corresponds to L^2D single-flip trials). Vapor films are clearly seen between the surfaces and the liquid. A predrying transition has thus occurred. For $L = 256$ and 512, these films develop within 1000 passes. In contrast, a system with $L = 16$ remains in the confined liquid phase after 20,000 passes. Evidently, the formation of the vapor films is driven by the growth of capillary-wave fluctuations. In Fig. 4, the average-density profiles for $L = 256$ and 512 are shown. The average vapor-film thickness $\bar{\ell}$ is determined by the relation [19]:

$$2\rho_g \bar{\ell} + \rho_l (D - 2\bar{\ell}) = \frac{1}{L^2} \sum_i n_i \tag{9}$$

The profile for $L = 512$ has a larger interfacial thickness ($\bar{\ell} = 1.97$) than for $L = 256$ ($\bar{\ell} = 1.80$). The difference is in accord with the estimation of film thickness from the thickness of a free interface (i.e., without surfaces), $\sim\sqrt{\ln L/2\pi\sigma_{gl}}$ [21].

If a vapor tube bridging the interfaces grows to a critical size, the system approaches its equilibrium gas state with an expanding vapor tube [7]. Thus, a plausible transition state for the evaporation coincides with two close-together vapor films connected by critically large tubes. Figure 5

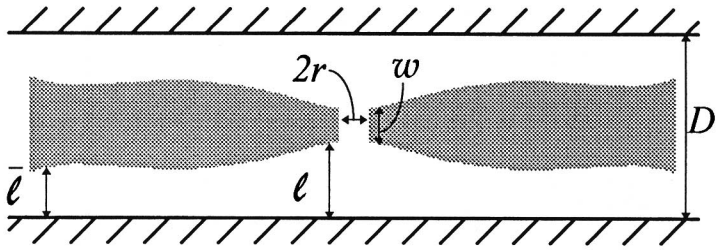

Fig. 5. Schematic depiction of the transition state. The critical vapor tube is of diameter $2r \sim w$ [Eq. (11a)].

shows a schematic interfacial configuration at this transition state. The free energy associated with the pictured fluctuation is approximately

$$\Delta F(r, \ell) = 2[\pi\sigma_{gl}(\ell - \bar{\ell})^2/2] + (2\pi\sigma_{gl} rw - 2\pi\sigma_{gl} r^2) \tag{10}$$

The first term corresponds to the free energy for bringing the two interfaces to a distance ℓ away from the surfaces. Here, we have assumed that the two interfaces are noninteracting. The second term is the free energy for forming a tube of radius r and length $w(=D-2\ell)$. At the saddle point of ΔF, the critical size of the vapor tube and the associated free energy barrier height are given by

$$2r_c = w_c = (D - 2\bar{\ell})/3 \qquad \text{and} \qquad \Delta F^{\ddagger} = \pi\sigma_{gl}(D - 2\bar{\ell})^2/6 \tag{11a}$$

When $\bar{\ell} \ll D/2$, the evaporation path is an activation-controlled process. The probability of reaching the transition state is given by

$$P^{\ddagger} \sim L^2 \exp(-\beta \Delta F^{\ddagger}) \tag{11b}$$

For systems with $L = 512$ and with $\bar{\ell} = 1.97$ after 10,000 passes, Eqs. (11) predict $w_c \sim 2.7$ and $P^{\ddagger} \sim 10^{-5}$. For $L = 256$, with $\bar{\ell} = 1.80$ after 70,000 passes, $P^{\ddagger} \sim 10^{-6}$.

The pathway for evaporation is very different for systems with periodic boundary conditions. For any such finite system, the long-time nature of the interfacial dynamics should correspond to quasi-one-dimensional diffusion [22(a)]. In this situation, the effective interface mobility is enhanced for small L [15, 22, 23]. With periodic boundary conditions and $L = 16$, we find that the confined system evaporates within 10,000 passes. In this case, the interfaces fluctuate freely into the thinning of the liquid film, and the decay of the metastable state is diffusion-driven.

Assuming the occurrence of evaporation obeys Poisson statistics, the mean lifetime of the metastable state should be $\sim 1/P^{\ddagger}$. The effects of transient vapor tubes [24] will lower $\Delta F^{\ddagger}$ and thus increase $P^{\ddagger}$ from what is given by Eqs. (11). In particular, the presence of a bridging vapor tube enhances the fluctuations that bring the interfaces close together. The probability of forming a single-column vapor tube across two interfaces separated by w is $P^{(1)}_{\text{tube}}(w) \propto \exp[-\beta\varepsilon(4w-2)/2]$. Decreasing interfacial separation therefore favors tube formation. This cooperative effect should be important when the system is close to the transition state. To take account of the film thickness which varies across the x–y direction, the system can be divided into columns of size ξ^2, where ξ is of the order of the bulk correlation length [19]. Let $P_c(w, t; L)$ be the probability that the column c having an average film thickness $w = \sum_{i \in c} n_i/\xi^2$ at time t. The probability of observing a narrow tube in the system at time t is given roughly by

$$\mathscr{R}_{\text{b}}(t; L) \sim L^2 \sum_{w} P_c(w, t; L)\, P^{(1)}_{\text{tube}}(w) \tag{12}$$

With $P_c(w, t; L)$ calculated from simulations, we find $\mathscr{R}_{\text{b}}(10^4; 512) \sim 10^{-3}$. For $L = 256$, $\mathscr{R}_{\text{b}}(10^4; 256) \sim 5 \times 10^{-5}$ and $\mathscr{R}_{\text{b}}(7 \times 10^4; 256) \sim 5 \times 10^{-4}$.

The evaporation process captured in our simulations is in accord with the above analysis. In the several runs we have performed for $L = 512$, the systems evaporate in 10,000 to 20,000 passes. The thin liquid film bounded by the two liquid–gas interfaces has an average thickness w of about eight lattice spacings. The film thickness fluctuates due to thermal excursions of the interfaces. Just before evaporation, the two interfaces are locally separated by about three lattice spacings and are bridged by a tube that then expands. The system with $L = 256$ remains in the metastable state up to 70,000 passes. This lengthening of evaporation time, from 10,000–20,000 passes to over 70,000 passes, is due to the diminished amplitude of capillary waves that occurs with the smaller system.

Capillary-wave fluctuations can also be suppressed by placing attractive sites on the surfaces. We have performed simulations on the inhomogeneous surfaces [7]. The simulation time required to observe evaporation in these systems is longer than for systems with uniform surfaces. Interfacial growth and fluctuations are hindered due to occasional pinning of the induced interfaces at the attractive sites. The interaction between the two liquid–gas interfaces that arises from bridging vapor tubes should be reduced according to Eq. (12). Additionally, the barrier height to reach the transition state increases according to Eq. (11a). The surface inhomogeneity may also reduce the prefactor in the expression for $P^{\ddagger}$ in Eq. (11b).

ACKNOWLEGDMENTS

This work was supported in part by a grant from the National Science Foundation (NSF), and an NSF graduate fellowship to one of us (K.L.). At the early stages, this work was also supported by the Office of Naval Research. During this time, the authors benefited from conversations with A. Luzar.

REFERENCES

1. R. Evans, *J. Phys. Condens. Matter* **2**:8989 (1990).
2. A. O. Parry and R. Evans, *Physica A* **181**:250 (1992).
3. H. K. Christenson and P. M. Claesson, *Science* **239**:390 (1988).
4. J. L. Parker, P. M. Claesson, and P. Attard, *J. Phys. Chem.* **98**:8468 (1994).
5. H. K. Christenson, J. Fang, and J. N. Israelachvili, *Phys. Rev. B* **39**:11750 (1989).
6. V. V. Yaminsky, V. S. Yushchenko, and E. D. Shchukin, *J. Colloid Interface Sci.* **96**:307 (1983).
7. K. Lum and A. Luzar, *Phys. Rev. E* **56**:6283 (1997).
8. R. Pandit and M. Wortis, *Phys. Rev. B* **25**:3226 (1982).
9. R. Pandit, M. Schick, and M. Wortis, *Phys. Rev. B* **26**:5112 (1982).
10. H. Nakanishi and M. E. Fisher, *J. Chem. Phys.* **78**:3279 (1983).
11. D. Nicolaides and R. Evans, *Phys. Rev. B* **39**:9336 (1989).
12. E. V. Albano, K. Binder, D. W. Heermann, and W. Paul, *Surf. Sci.* **223**:15 (1989).
13. K. Binder and D. P. Landau, *J. Chem. Phys.* **96**:1444 (1992).
14. K. Binder, D. P. Landau, and A. M. Ferrenberg, *Phys. Rev. E* **51**:2823 (1995).
15. K. Binder and D. P. Landau, *Phys. Rev. B* **37**:1745 (1988).
16. J. D. Weeks, *Phys. Rev. Lett.* **75**:2694 (1995).
17. K. K. Mon, D. P. Landau, and D. Stauffer, *Phys. Rev. B* **42**:545 (1990). (There, MC estimates give $\varepsilon/k_B T_R \approx 1.6358$.)
18. F. Buff, R. A. Lovett and F. H. Stillinger, *Phys. Rev. Lett.* **15**:621 (1965).
19. J. D. Weeks, *J. Chem. Phys.* **67**:3106 (1977).
20. L. Monette, A. J. Liu, and G. S. Grest, *Phys. Rev. A* **46**:7664 (1992).
21. See, e.g., S. K. Ma, *Statistical Mechanics* (World Scientific, Philadelphia, Singapore, 1985).
22. (a) K. K. Mon, K. Binder and D. P. Landau, *Phys. Rev. B* **35**:3683 (1987); (b) K. K. Mon, K. Binder, and D. P. Landau, *J. Appl. Phys.* **61**:4409 (1987).
23. D. B. Abraham and P. J. Upton, *Phys. Rev. B* **39**:736 (1989).
24. M. E. Fisher and D. S. Fisher, *Phys. Rev. B* **25**:25 (1982).